PAPER

Check for updates

Acceleration characteristics of a macroscopic contact line induced by interactions of a liquid film with micro spheres

Luyuan Gong,[a] Chengtao Yan [iD][a] and Lizhong Mu*[ab]

It has been reported that a rapid acceleration of a macroscopic contact line (MCL) during droplet spreading is induced by particles deposited on a hydrophilic surface. In this study, we quantitatively correlated the MCL acceleration with the size of a single sphere during the rapid motion of a liquid film on a silicon wafer or glass surface. A sphere coated with gold was used in our experiments. Power law relationships were identified between the maximum velocity and the acceleration period, as well as between the acceleration period and the initial velocity at which the MCL contacted the sphere. In addition, the acceleration period increases linearly with sphere diameter. In the acceleration period, the spreading distance of the liquid film from the liquid front to the particle centre was proportional to the diameter of the sphere. This study provides detailed information on the dynamics of MCL acceleration during liquid spreading in the presence of micro particle interactions on a smooth hydrophilic surface. The findings will be helpful for improving the wetting performance in micro devices.

1. Introduction

Wetting a solid with a liquid is a common natural phenomenon, frequently encountered in industrial settings and daily life. Free surface film flows, a typical example of wetting phenomena, occur regularly during coating and cooling processes in a broad range of industrial applications. A comprehensive understanding of the dynamics and control of the wetting behaviour is essential for the effective transportation of fluids under microgravity or in the micro device.[1–3]

When a drop is deposited on a smooth hydrophilic substrate, two wetting regimes exist: the droplet either spreads completely or remains stuck in place. These two regimes are distinguished by the spreading parameter S, which is expressed by the interfacial tension.[3–6] The drop can spread with unbalanced interfacial tension until it is close to its equilibrium. There are two wetting processes: an initial inertia-dominated phase[7–10] and a viscosity-dominated process phase.[8–13] The power law relationship between the spreading radius and time has been previously characterised by scholars.[10–15] In the inertial regime, the spreading radius r scales as $r \sim t^{1/2}$ while in the viscous regime, the droplet spreading follows Tanner's law[10–14] if r is

smaller than the capillary length $l_c = (\gamma/\rho g)^{1/10}$. When $r \geq l_c$, the spreading radius r scales as $r \sim t^{1/8}$.[14,15] Mitra *et al.*[11] found that the drop spreading radius scales as $r \sim t$ in the beginning of drop spreading driven by viscosity. This initial viscosity-driven phase either lasts during the entire spreading or switches to an intermediate inertial process with the scaling of $r \sim t^{1/2}$.

When a liquid spreads on a structured surface, the liquid front will be pinned in a short time because of the existence of structures on the solid surface at the early stage.[16–21] Fast propagation processes have been detected.[14–20] In particular, when the droplet is spreading towards a moveable particle and the capillary number Ca is larger than 5×10^{-4}, the particle will be sucked into the liquid. The capillary number Ca is given by Ca $= \mu V_0/\gamma$, where μ is the dynamic viscosity, V_0 is the MCL velocity when the liquid front makes contact with the particle and γ is the surface tension. When the capillary number is on the order of 10^{-6}, the particle induces a sharp acceleration of the liquid front.[22–24] In their research, a theoretical model was developed with an assumption of the axisymmetric meniscus formation around the particle and the immediate relaxation of the Laplace pressure during the liquid–particle interaction. They predicted a power law behaviour of the MCL velocity V at the late stage of liquid–particle interaction: $V \sim t^{-3/4}$. And they obtained a scaling law for the acceleration time, $t_{max} \sim L^{7(1-k)/6k}$, where k is dependent on the relation between the spreading radius r and capillary length l_c. They also predicted the acceleration time t_{max} and the particle radius a, $t_{max} = 0.074a$. However, these correlations were not experimentally validated when the droplet spreads

[a] *Key Laboratory of Ocean Energy Utilization and Energy Conservation of Ministry of Education, School of Energy and Power Engineering, Dalian University of Technology, 116024 Dalian, China. E-mail: muliz@dlut.edu.cn*

[b] *Department of Mechanical Engineering, Faculty of Science and Technology, Tokyo University of Science, Japan*

on other hydrophilic surfaces. And there is little information concerning the correlation of the acceleration characteristics of MCL with the size of a single micro sphere on different solid surfaces. It is worth noting that previous studies have demonstrated how the presence of micro-objects arranged in different geometric shapes affects wetting.[24] Additionally, three distinct regimes of MCL behavior have been identified across different ranges of capillary numbers.[25] Later, the study explores the pressure and velocity fields within the liquid film, as well as how particle-liquid interactions influence local flow characteristics.[21] Through numerical simulations, the pumping effect of the heterogeneous meniscus formed around spherical particles has been investigated. Overall, previous work has primarily focused on the phenomenon of particle-induced liquid film flow, with limited research on the differences in MCL kinetic characteristics under varying microsphere parameters.

The focus of this study is to quantitatively correlate the MCL acceleration caused by the interaction of particles and liquid films with the size of microspheres. It guides optimizing hydrophilic surface wettability *via* particle size adjustment. Understanding droplet wetting dynamics on hydrophilic surfaces, particularly influenced by microspheres, is key for microfluidic system design and microdevice performance enhancement. This is crucial for applications like drug delivery and chemical sensing, where precise fluid control is essential.

2. Experiments

A droplet of silicone oil of volume $\Omega = 2$ mm^3 was deposited on the two different horizontal surfaces: silicon wafer and glass.
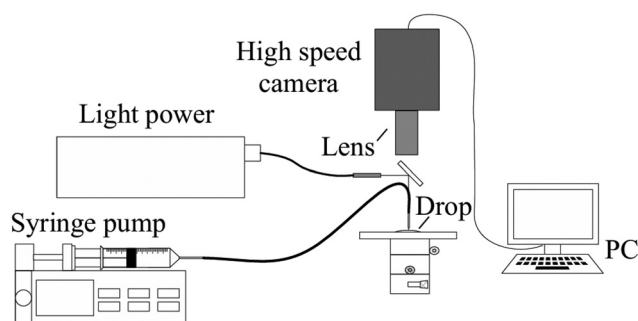

Fig. 1 Schematic of the experimental apparatus. The high-speed camera had a resolution of 1028×728 pixels and a frame rate up to 250 frames per second (fps). The distance between the needle and the substrate was 2.0 mm. The needles of the syringe pumps are treated with a fluorinated compound to create a hydrophobic surface.

The droplet was generated by a syringe pump connected to a hypodermic needle. Prior to each experiment, the substrate was cleaned with acetone and a plasma cleaner (Harrick, PDC-32G) for 10 min. Next, spheres with different diameters were placed on the substrate at a given distance of $L \geq 4$ mm from the needle location. An optical system was used to observe the motion of the droplet spreading on the smooth solid surface (Fig. 1). The system included a high-speed camera with an objective lens ($500\times$ magnification).[26] The dynamic parameters of MCL are obtained by the corresponding high-speed camera software. The specific measurement process is as follows: (1) import the images into the analysis software. (2) Convert pixel distance to actual distance using a scale. (3) Track the center point of the MCL. (4) Export the data on velocity, distance, and time from the tracking process. The physical properties of the spheres, silicon oil, and substrates are listed in Table 1.

3. Results and discussion

Fig. 2 shows time-sequence images of a droplet spreading on the silicon wafer with and without a sphere, and on the glass with the sphere deposited ahead of the liquid front. The yellow dotted line represents the position of the MCL at $t = t_0$, and the particle location. Comparing Fig. 2(a)–(c) shows the rapid propagation of the MCL ($t_0 + 4$–6 s) after the pinning of the MCL by the particle ($t_0 + 2$ s), as reported by Mu *et al.*[22]

Fig. 3a shows the comparison of the velocity of MCL propagation with and without liquid–sphere interaction on the silicon wafer and glass surface. A clear period of velocity acceleration (the part of the period with a large speed change to the left of the dotted line, the moment at the end of the obvious acceleration phase, is defined as t_{max} and shown in Fig. 3a) was observed after the interaction of the MCL with the particle. Immediately after reaching the maximum velocity V_{max}, the velocity of the MCL begins to decay with time. When the liquid made contact with the particle, the velocity was defined as initial velocity V_0. We found similar patterns in the stages of acceleration and decay for the droplets spreading on the different solid surfaces.

The causes of this phenomenon are analyzed. Firstly, microspheres alter the local surface tension and capillary forces at the liquid–solid interface. This change increases the driving force for the macroscopic contact line (MCL), leading to acceleration. Secondly, the interaction between the liquid and microspheres generates complex flow patterns and vortices

Table 1 Physical properties of the sphere and silicon oil on different solid surfaces

Silicon oil[a]	Density [kg m^{-3}]	873				
	Kinematic viscosity [mm^2 s^{-1}]	2.0				
	Surface tension at 25 °C [mN m^{-1}]	18.3				
Spherical particle[b]	Diameter of sphere d [μm]	10	20	30	40	50
	Density $\times 10^{-3}$ [kg m^{-3}]	2.05	1.64	1.60	1.55	1.47
Substrate	Silicon wafer[c], glass[d]					

[a] Polydimethylsiloxane, KF-96L-2cSt, Shin-Etsu Chemical Co., Ltd. [b] Gold nickel alloy coated acrylic particles. [c] Roughness $\leq$ 10 nm, Shin-Etsu Chemical Co., Ltd. [d] Roughness $\leq$ 0.2 nm, Shin-Etsu Chemical Co., Ltd.
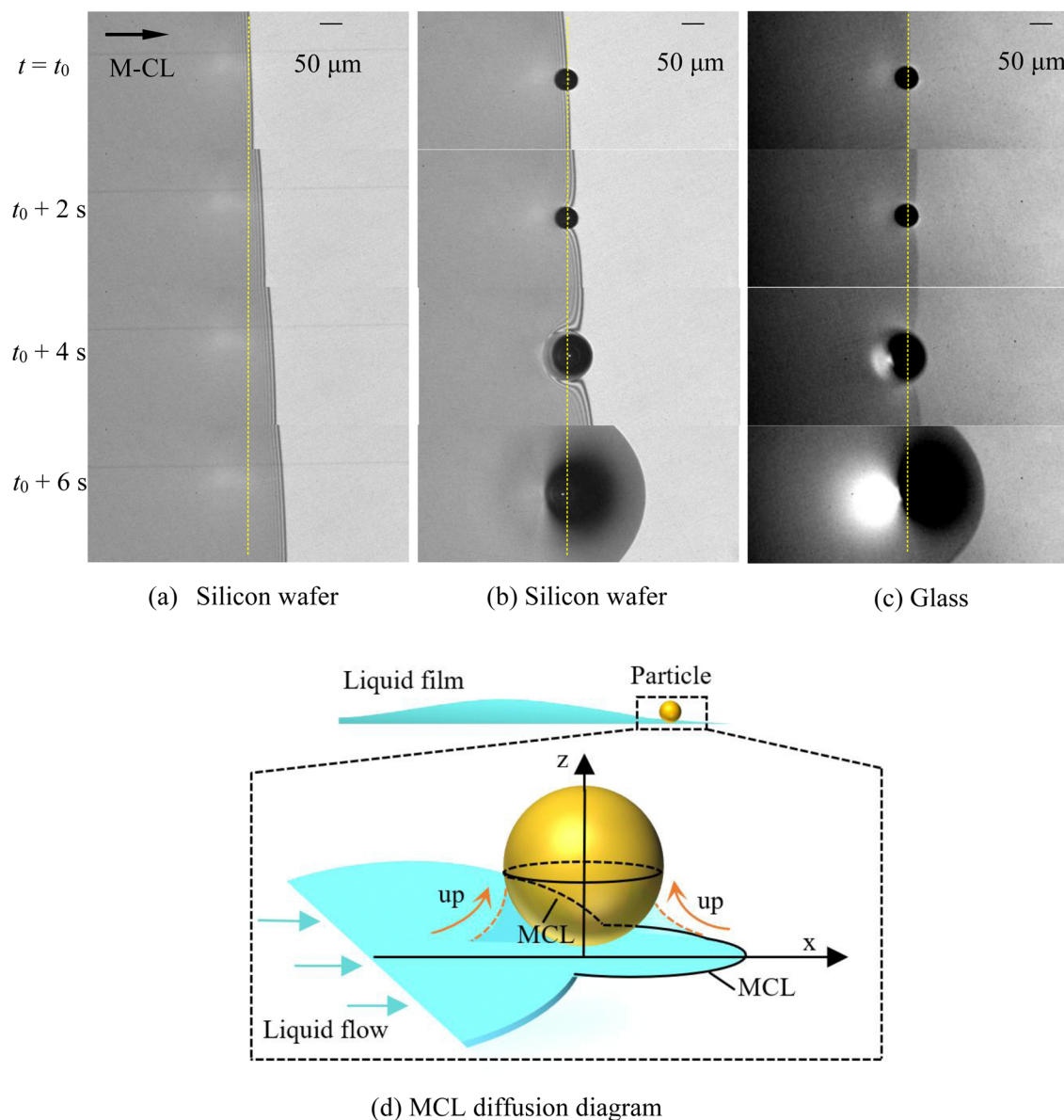
Fig. 2 Time sequence of droplet spreading movements (a) on the silicon wafer without the particle, (b) on the silicon wafer with a sphere and (c) on the glass with a sphere. The yellow line marks the location of the MCL at $t = t_0$. The direction of the MCL is shown as the arrow. Scale bar: 50 μm. (d) MCL diffusion diagram.

near the contact line. These patterns enhance liquid transport, speeding up the spreading rate. Lastly, when the MCL contacts metal particles, the metal surface exerts an adhesive force on the liquid film, altering its surface tension and creating a Laplace pressure difference within the fluid. These forces drive the liquid film towards the metal particles.

Fig. 3b shows the spreading distance of the MCL over time after the interaction. The y-axis shows the spreading distance $x - x_0$ from the centre of the sphere to the location of the MCL (Fig. 3b inset). The x-axis gives the elapsed time $t - t_0$ after the interaction. During the acceleration period $0 \sim t_{max}$, the spreading distance from the liquid front to the particle centre was defined as l_{max}. It can be seen that the sphere size significantly affects the acceleration behaviour during the liquid–particle interactions; as the

sphere radius decreased, both the acceleration period and acceleration distance decrease accordingly.

To quantitatively examine the acceleration characteristics and also the dependence of acceleration on the particle diameter d in the liquid–particle interactions, the maximum velocity V_{max}, initial velocity V_0, acceleration period t_{max}, and acceleration distance l_{max} were employed to describe the rapid MCL acceleration.

Fig. 4 illustrates the correlations between t_{max}, V_0 and V_{max} during the acceleration of the MCL induced by the interaction with spheres of different sizes on the silicon wafer. As presented in Fig. 4(a), there is a power law relation between t_{max} and V_0. The dotted line shows the curve fitting relation of $t_{max} \sim V_0^{\alpha}$, with $\alpha = -1.18$, which can be deduced from the work of Mu et al.[22] They derived a scaling law for the acceleration
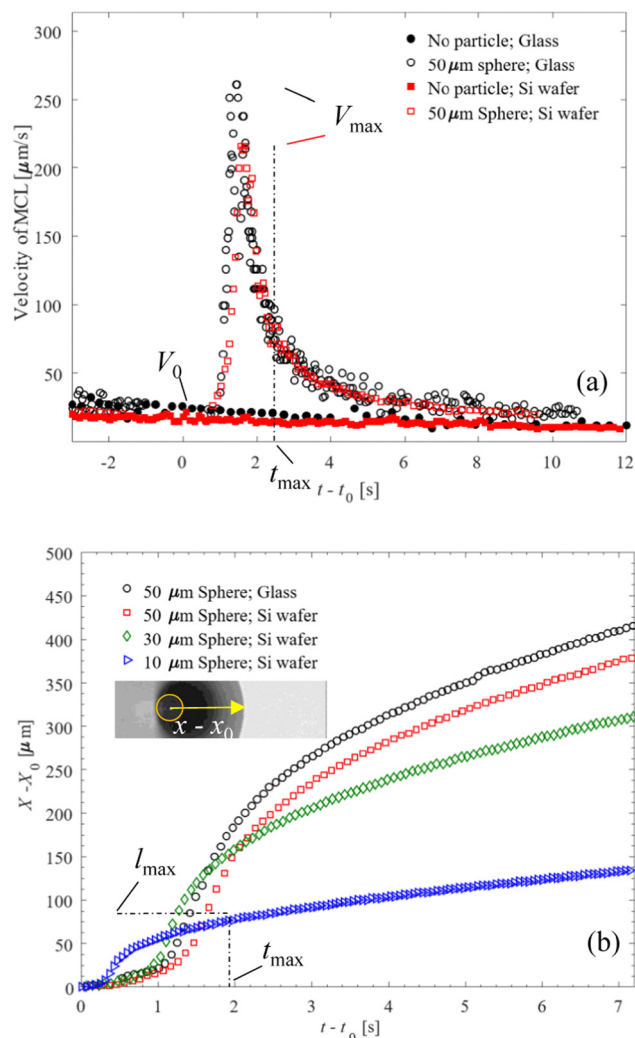
Fig. 3 (a) Velocity distribution of the MCL over time with and without sphere interaction on the silicon wafer and glass surface. The diameter of the sphere was 50 μm. V_0 was defined as the velocity of the MCL when it made contact with the particle at $t = t_0$. (b) Spreading distance as a function of time after interaction with spheres of different sizes. The inset shows the distance between the MCL location and the centre of the sphere.

time t_{max}, $t_{max} \sim L^{7(1-k)/6k}$, by considering the slow liquid supply from the bulk drop to the meniscus and the volume transportation in the free spreading of a drop, where L is the distance between the needle and the sphere. In our experiments, k equals to 1/8 on account of the fact that the spreading radius is larger than the capillary length l_c. Some published works[15,22] have reported a power law relation for the spreading radius R, $R \sim t^{1/8}$, where t is the time elapsed. We can drive a relation of spreading radius with velocity. When the liquid film made contact with the sphere, the spreading radius R is equal to the distance L, and the velocity is just defined as the initial velocity V_0. The exponent α was then estimated with the value of -1.18 (Fig. 4a). In Fig. 4b, a power law relation is also observed for V_{max}, where $V_{max} \sim t_{max}^{\beta}$. Based on the theory of dimension analysis, the exponent $\beta = 1/\alpha \sim -0.85$ was obtained, as the dotted line showed in Fig. 4b.
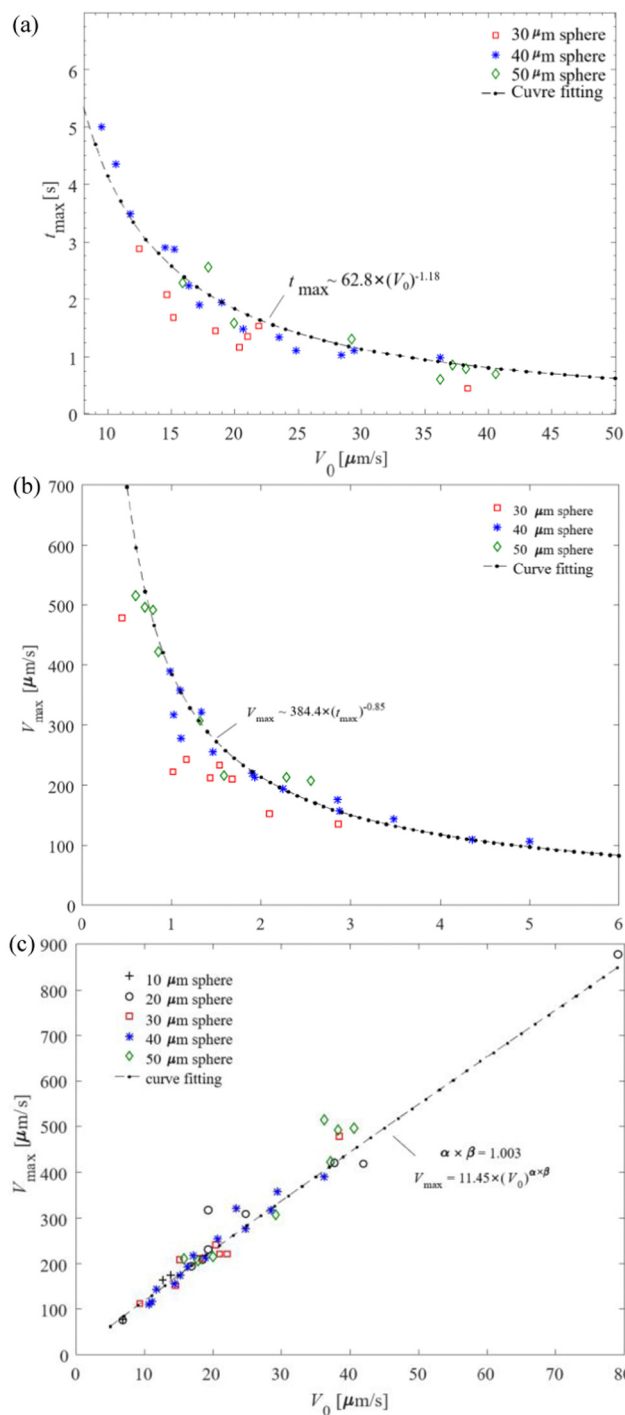

Fig. 4 Relations among t_{max}, V_0 and V_{max} during the accelerated motion of the MCL on the silicon wafer.

For the droplet spreading on the silicon wafer, V_{max} is almost 11 times larger than V_0, as shown by the dotted line in Fig. 4c. Previous studies have reported that the ratio of V_{max}/V_0 tends to remain relatively constant.[22,24] Fig. 5 illustrates the ratio of V_{max} to V_0 for spheres with different sizes on the silicon wafer and glass surface. The ratio is larger when the droplet spreads on the glass than the silicon wafer. On average, the ratios are approximately 11.0 for wafer and 11.5 for glass.
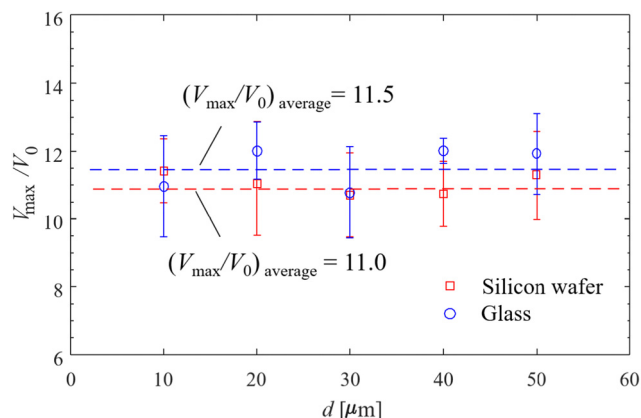
Fig. 5 Ratio of V_{max} to V_0 as a function of particle diameter. The red and blue dotted lines represent the average of V_{max}/V_0. For the silicon wafer surface, the average ratio was 11.0, and for the glass surface it was 11.5.

We observed that the surface roughness is different between the glass substrate and silicon wafer used in our experiments. It had been proved that the surface roughness significantly affects the liquid motions.[24] Rough surfaces increase the frictional resistance between the fluid and the wall, leading to greater resistance in liquid film flow. This is because the presence of roughness requires the fluid to overcome more surface irregularities, thereby increasing energy consumption. The direction and magnitude of roughness affect the flow velocity of the liquid film. If the roughness is aligned with the flow direction, it may reduce the contact area between the fluid and the solid, thereby increasing the flow velocity. Conversely, if the roughness is perpendicular to the flow direction, it will decrease the flow velocity. The description in Fig. 2 already indicates that the roughness of the silicon ≤ 10 nm, and the roughness of the glass substrate ≤ 0.2 nm. This is also the reason for the slight differences in the ratio of V_{max} to V_0 on the silicon and glass substrates.

The correlation of the acceleration period t_{max} with the sphere diameters is shown in Fig. 6. It can be seen that the acceleration period seems to linearly increase with the size of
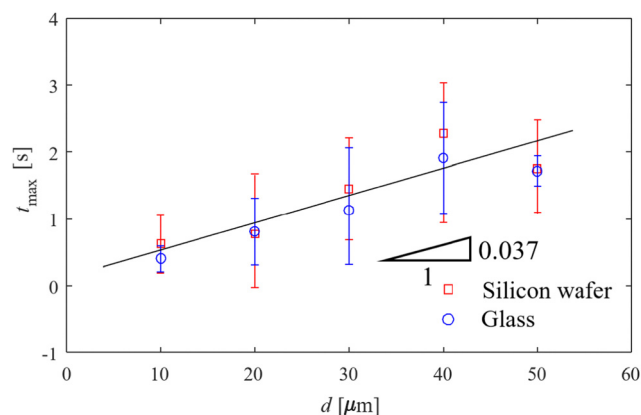

Fig. 6 Relation between the acceleration period t_{max} and sphere diameter d on silicon and glass surfaces. The straight line shows a linear fit $t_{max} = 0.037d$, which has been reported previously.[24]
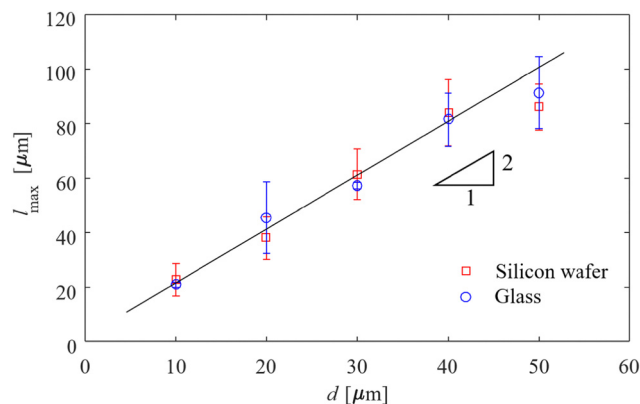

Fig. 7 Accelerated distance l_{max} as a function of particle diameter d. The straight line shows a linear fit $l_{max} = 2.0d$.

the sphere on the two solid surfaces. A linear fit of $t_{max} = 0.037d$ was predicted by Mu *et al.*[24] No significant difference was observed between the droplet spreading on the silicon wafer and glass surfaces.

Fig. 7 illustrates how the acceleration distance l_{max} on the two solid surfaces varied with sphere diameter. The straight line represents a linear fit, $l_{max} = 2.0d$, indicating that the accelerated distance is proportional to the sphere diameter. The slope of the linear correlation is nearly identical for droplet spreading on both the silicon wafer and glass surfaces.

As reported in the work of Mu *et al.*,[24] the successive linear liquid–particle interactions can enhance the liquid film propagation and the speed of wetting. Combined with the result in Fig. 7, if the spheres are deposited on the solid surface with an inter particle distance of $2d$ in a linear arrangement of spheres, the motion of the liquid will be enhanced to the greatest extent. This will be useful for designing the most efficient arrangement for MCL motion or wetting on a hydrophilic surface.

4. Conclusions

We quantitatively investigated the acceleration behaviour of droplet spreading induced by an interaction with a single sphere of different sizes on a hydrophilic surface. Through curve fitting, we identified power law relations between V_{max} or V_0 with t_{max} for droplet spreading on a silicon wafer. It is found that the acceleration period t_{max} and the acceleration diffusion distance l_{max} increase linearly with the increase of the sphere size. Moreover, the acceleration and decay stages of droplet diffusion on different solid surfaces show similar rules. When the ball is deposited on the solid surface in a straight line arrangement and the particle spacing is $2d$, the liquid movement will be enhanced to the greatest extent. This study provides detailed knowledge about the acceleration of MCL spreading that is induced by a spherical particle on a smooth substrate. Offering useful guidance for the efficient designation of surface structure to optimize wetting on hydrophilic surfaces.

There are some limitations to this study. Theoretical explanations remain to be developed, such as why the accelerated

distance was proportional to sphere diameter. The sphere diameters were limited to a ranged of 10–50 μm, and the influence of particle materials on the acceleration behaviour was not consider. It has been shown that different particle structures have different effects on the accelerating behavior of liquid film spreading. If the optimization methods are combined, a particle structure that is most conducive to wetting can be obtained. The optimization of particle configuration that accelerates the wetting of solid surface will be a potential research direction.[27] We are currently working on further studies of these topics.

Author contributions

Luyuan Gong: funding acquisition (equal); methodology (equal); project administration (equal); writing – review & editing (equal). Chengtao Yan: conceptualization (equal); data curation (equal); methodology (equal); writing – original draft (equal). Lizhong Mu: funding acquisition (equal); investigation (equal); resources (equal).

Data availability

The authors confirm that the data supporting the findings of this study are available within the article.

Conflicts of interest

We confirm that there are no known conflicts of interest associated with this publication and there has been no significant financial support for this work that could have influenced its outcome.

Acknowledgements

References

1 D. Bonn, J. Eggers, J. Indekeu, J. Meunier and E. Rolley, Wetting and spreading, *Rev. Morden Phys.*, 2009, **81**(2), 739–805.

2 H. Bo, Y. Wu, L. Guang and J. Huang, Contact line-based model for the Cassie-Wenzel transition of a sessile droplet on the hydrophobic micropillar-structured surfaces, *Appl. Surf. Sci.*, 2021, **542**, 148611.

3 Z. Wang, L. Li and M. Yang, Molecular dynamics simulation of the wetting characteristics of a nanofluid droplet on rough substrate, *J. Mol. Liq.*, 2020, **319**, 114204.

4 G. Liu, Y. Li, W. Long, X. Hu, J. Cao and M. Yan, Wetting kinetics and spreading phenomena of the precursor film and bulk liquid in the AgCuTi/TC4 system, *J. Alloys Compd.*, 2019, **802**, 345–354.

5 A. Vieira, W. Cui, V. Jokinen and H. A. Robin, Through-drop Imaging of Moving Contact Lines on Opaque Surfaces, *Soft Matter*, 2023, **19**(13), 2350–2359.

6 Z. Fan, D. Liu, S. Pan, J. Ma and X. Chen, Spreading dynamics of the viscous droplet impacting on a spherical particle, *Phys. Fluids*, 2023, **35**(2), 023311.

7 R. Bernard, D. Baumgartner, G. Brenn, C. Planchette, B. Weigand and G. Lamanna, Miscibility and wettability: how interfacial tension influences droplet impact onto thin wall films, *J. Fluid Mech.*, 2021, **908**, A36.

8 M. Kansal, V. Bertin, C. Datt, J. Eggers and J. H. Snoeijer, Viscoelastic wetting: Cox–Voinov theory with normal stress effects, *J. Fluid Mech.*, 2024, **985**, A17.

9 H. Bao, D. Wang, F. Ren, L. Bao and V. Nikolai, A comparative analysis of the effective and local slip lengths for liquid flows over a trapped nanobubble, *Int. J. Multiphase Flow*, 2018, **104**, 166–173.

10 R. Saiseau, C. Pedersen and A. Benjana, *et al.*, Near-critical spreading of droplets, *Nat. Commun.*, 2022, **13**(1), 7442.

11 E. Julien, S. M. Rubinstein and S. Care, Slow spreading with a large contact angle on hygroscopic materials., *Soft Matter*, 2023, **19**, 3475–3486.

12 I. Yoon, S. Shin and D. Juric, *et al.*, Numerical investigation of spreading time in droplet impact with a large spherical surface: from physical analysis to data-driven prediction model., *Theor. Comput. Fluid Dyn.*, 2024, **8**, 225–250.

13 M. J. De Ruijter, J. De Coninck and G. Oshanin, Droplet spreading: partial wetting regime revisited, *Langmuir*, 1999, **15**, 2209–2216.

14 B. M. Jose, D. Nandyala and T. Cubaud, *et al.*, Physical ageing of spreading droplets in a viscous ambient phase, *Sci. Rep.*, 2018, **8**, 14159.

15 A. Mesbahi, T. Germain, P. K. Patel, A. Putnam and Y. Karin, Tuning the fluid wetting dynamics on gold microstructures using photoactive compounds, *Appl. Surf. Sci.*, 2022, **589**, 152924.

16 P. De Gennes, Wetting: statics and dynamics, *Rev. Morden Phys.*, 1985, **57**, 827–863.

17 H. Nakamura, V. Delafosse, G. F. Dietze, L. Mu and T. Tsukahara, *et al.*, Enhancement of Meniscus Pump by Multiple Particles, *Langmuir*, 2020, **36**(16), 4447–4453.

18 M. S. Sadullah and J. R. Pantera, Factors controlling the pinning force of liquid droplets on liquid infused surfaces, *Soft Matter*, 2020, **16**(35), 8114–8121.

19 M. Zhou, J. Yu, J. Li, B. Wu and W. Zhang, Wetting induced fluid spread on structured surfaces at micro scale, *Appl. Surf. Sci.*, 2012, **258**(19), 7596–7600.

20 Y. Wang, X. Luo, W. Qin and F. Jiao, New insights into the contact angle and formation process of nanobubbles based on line tension and pinning, *Appl. Surf. Sci.*, 2019, **481**, 1585–1594.

21 H. Nakamura, T. Ogawa, M. Inoue, L. Mu and N. Harunori, *et al.*, Pumping effect of heterogeneous meniscus formed around spherical particle, *J. Colloid Interface Sci.*, 2020, **562**, 133–141.

22 L. Mu, D. Kondo, M. Inoue, T. Kaneko, H. N. Yoshikawa, F. Zoueshtiagh and I. Ueno, Sharp acceleration of a macroscopic contact line induced by a particle, *J. Fluid Mech.*, 2017, **830**, R1.

23 H. H. Wei, H. K. Tsao and K. C. Chu, Slipping moving contact lines: critical roles of de Gennes's 'foot' in dynamic wetting, *J. Fluid Mech.*, 2019, **873**, 110–150.

24 L. Mu, H. N. Yoshikawa, D. Kondo, T. Ogawa, M. Kiriki, F. Zoueshtiagh, M. Motosuke, T. Kaneko and I. Ueno, Control of local wetting by microscopic particles, *Colloids Surf., A*, 2018, **555**, 615–620.

25 D. Kondo, L. Mu, F. de Miollis, T. Ogawa, M. Inoue, T. Kaneko, T. Tsukahara, H. Yoshikawa, F. Zoueshtiagh and I. Ueno, Acceleration of the macroscopic contact line of a Droplet spreading on a substrate after interaction with a particle, *Int. J. Microgravity Sci. Appl.*, 2017, **34**, 350405.

26 W. Bo, Z. Shiyang, H. Peng, B. Xiangju, D. Kaifan, C. Bingquan, M. Xiangtao and C. Y. J., Buckling of quasi-perfect cylindrical shell under axial compression: A combined experimental and numerical investigation, *Int. J. Solids Struct.*, 2018, **130–131**, 232–247.

27 P. Hao, Y. Wang, C. Liu, B. Wang and H. Wu, A novel non-probabilistic reliability-based design optimization algorithm using enhanced chaos control method, *Comput. Methods Appl. Mech. Eng.*, 2017, **318**, 572–593.